A Method to Enable Reduced Sensor Capacitor Voltage Estimation in Modular Multilevel Converters

Eugene Tinjinui Ndoh[a*], Seongsu Byeon[a], Lotz Marc[b] and Soeren Ehlers[a]

[a] DLR Institute for Maritime Energy Systems, Geesthacht, Germany
[b] Technische Universität Braunschweig, Braunschweig, Germany
*eugene.ndoh@dlr.de

Abstract

Bulk power applications such as shipping increasingly consider multilevel converter topologies such as modular multilevel converters (MMC), which offers the advantages of scalability, good power quality, and reconfigurability. The internal functioning of MMC requires complete knowledge of the capacitor voltages that make up their submodules meaning a large number of sensors are needed and thus a high number of potential points of failure exist. To increase reliability and reduce investment costs, state estimation techniques such as KALMAN filters have been employed to replace the physical sensors. Analytical techniques based on the knowledge of arm current, arm voltage, and submodule states have also been developed. These techniques exploit the fact that at an insertion index of 1, the arm voltage equals the capacitor voltage on the submodule which permits the estimation algorithm to refresh periodically with measured data thereby increasing the accuracy. This method requires a long refresher time, especially when many submodules are used per arm. In this study, we propose an improved analytical estimation by not only using unity insertion indices, but also exploiting transitions between two successive insertion indices. The study was carried out on a 4 submodule per arm MMC system. The estimated capacitor voltages were then compared with sensor-based voltage measurements confirming the validity of the proposed method. It was then integrated into a complete MMC controller including the inner controls such as circulating current and capacitor voltage balancing.

Keywords: Modular Multilevel Converter, Insertion Index, Modulation index, Capacitor Voltage balancing, Circulating Current.

1. INTRODUCTION

The shipping industry is currently facing the challenge of achieving its climate goals through the adoption of new technologies. The electrification of ships is a critical factor in this regard, as it permits better integration of renewable energy and energy storage into the ship energy mix. Both academia and industry are seeking feasible ways to enable zero-emissions shipping. While direct current (DC) systems have shown benefits over conventional alternating current (AC) systems, their deployment has been limited to low-voltage direct current (LVDC) systems for small vessels, such as offshore support and inland vessels. To enable true DC transition in shipping, medium-voltage direct current (MVDC) systems [1] need to be developed, as the current electrical propulsion systems for large commercial vessels are based on medium-voltage alternating current (MVAC).

Modular Multilevel Converters (MMC) have been identified as the most promising power converter topology for medium-voltage direct current (MVDC) systems for large commercial vessels [2]. The full-bridge topology of MMC enhances the fault-limiting capabilities of shipboard power systems, which is one of the most critical design criteria for MVDC systems. Additionally, MMC offer modularity, flexible voltage levels, and low harmonic output voltages. However, one of the drawbacks of MMC is the high number of sensors required to measure numerous parameters, such as both AC and DC voltages/currents, arm currents, and capacitor voltages [3]. The high number of sensors lead to increase in the system size and cost as well as a reduction of the reliability. The sensors for capacitor voltage measurements account for a large portion of these sensors. Various studies have been conducted to address this challenge by adapting numerous estimation techniques for capacitor voltage estimation that could replace conventional sensors.

In this study, we propose an improved capacitor voltage estimation method for a grid tied MMC ship systems. Instead of utilizing a unity insertion index, the proposed method exploits the transitions between two successive insertion indices. In effect, insertion indices under normal operation change in steps of one. Knowing the changes in arm voltage,

DOI: https://doi.org/10.59490/ moses.2023.672

the arm currents as well as the state changes of the switches at the transition points permit capacitor voltage calculation. Analytical equations permit the estimation of the voltages between the transition instances. Given that state transitions occur throughout the period, the refreshing time for the proposed voltage estimation is shorter.

The rest of the paper is structured as follows: Section 2 provides an overview of the MMC topology, and control systems, Section 3 describes the state-of-the-art voltage estimation methods, Section 4 describes the proposed voltage estimation method, Section 5 presents the simulation results and an analysis of the obtained outcomes. Finally, in Section 6, the paper concludes with a summary of the main findings, a discussion of their implications, and possible future research directions.

2. MODELLING OF THE MMC

2.1. Topology descriptions

Figure 1 shows the architecture of a three-phase MMC consisting of half-bridge (HB) submodules. The MMC's DC bus or DC link are connected to the positive and negative bars of the three converter legs (a, b, c), each of which is made up of two arms. The arm connected to the positive bar is referred to as the upper arm (u), and the arm connected to the negative bar is referred to as the lower arm (l). Each arm contains a group of submodules (SM) and an inductor (L_{arm}). The inductor for each arm is serially linked to the arm SM group to reduce circulating currents arising from voltage disparities between the arms.

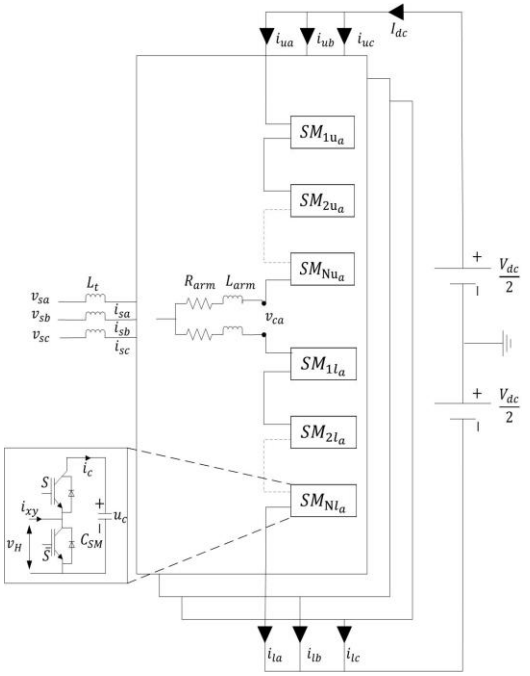

Figure 1: MMC architecture with HB submodule

Several types of MMC submodules [12] have been developed in the last few decades, such as Half-bridge and the Full-bridge submodules. The half-bridge (HB) submodule is often referred to as a chopper cell. It is composed of two MOSFET or IGBT switching devices with antiparallel diodes ($S\ and\ \overline{S}$) and a capacitor (C_{SM}). The two switching devices are operated in a complementary manner to regulate the capacitor voltage at a value of u_C. The capacitor voltage is given by:

$$u_c = \frac{1}{C}\int_{0+}^{t} i_c(t)\,dt \tag{1}$$

The capacitor current (i_c) in terms of the arm current (i_{xy}) and the switching state, S, is given by

$$i_c = S\, i_{xy} \tag{2}$$

Depending on the state of the top switch, the effect on the capacitor voltage for different directions of the arm current are listed in Table 1. The output voltage of the HB has two voltage levels, "0" and "u_c". When the top switch is "on", the output voltage is equal to u_c. In this mode, the capacitor voltage increases for positive arm currents and decreases for negative arm currents. When the top switch is "off", the output voltage is equal to "0", In this mode, the capacitor voltage remains constant, irrespective of the current direction. The output voltage of the HB can be represented in terms of the voltage and switching state of the top switch as $v_H = S\, u_c$.

S	v_H	i_{xy} >0	i_{xy} ≤0
1	u_c	$u_c \uparrow$	$u_c \downarrow$
0	0	$u_c \approx$	$u_c \approx$

Table 1. Switching states of HB SM

2.2. Modelling of the MMC

In Figure 2, the MMC is modelled using variable arm voltages, which are determined based on the states of the SMs and their corresponding capacitor voltages. In this study, an MMC inverter connected to a strong ship grid is considered. All three phases are controlled to inject balanced power into the grid, and normal operation (no fault) is assumed.

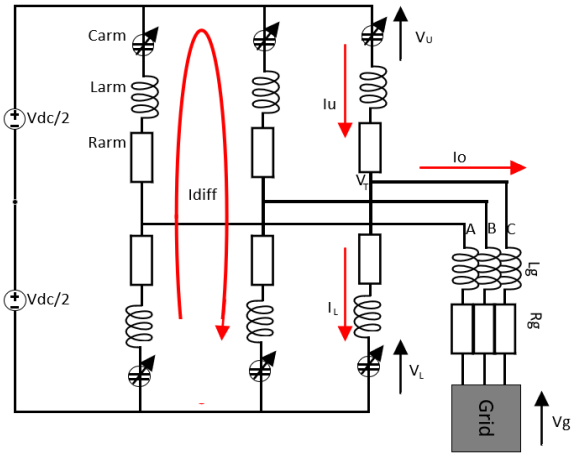

Figure 2: MMC single line diagram

In particular, for one phase, equation (3) and (4) can be established.

$$\frac{V_{dc}}{2} - V_U = V_T + \left(R_{arm} * I_U + L_{arm}\frac{dI_U}{dt}\right) \quad (3)$$

$$\frac{V_{dc}}{2} - V_L = -V_T + \left(R_{arm} * I_L + L_{arm}\frac{dI_L}{dt}\right) \quad (4)$$

As seen in equations (5) and (6) the arm currents consist of a DC component, an AC component, and a second-harmonic component known as the circulating current (I_{cc}). This circulating current flows between the arms and is caused by the differential voltages on each arm, resulting from their distinct switching patterns. The differential Current (I_{diff}) is the sum of the DC and second harmonic current.

$$I_U = \frac{I_{dc}}{3} + I_{cc} + \frac{I_o}{2} \quad (5)$$

$$I_L = \frac{I_{dc}}{3} + I_{cc} - \frac{I_o}{2} \quad (6)$$

I_{dc} represents the current from the DC link. Adding and subtracting equation (5) from equation (6) yields equation (7) and (8), respectively.

$$I_o = I_U - I_L \quad (7)$$

$$I_U + I_L = 2 * \left(\frac{I_{dc}}{3} + I_{cc}\right) = 2 * I_{diff} \quad (8)$$

By subtracting and adding equations (3) and (4), equations (9) and (10) are derived.

$$V_T = \left(\frac{-V_U + V_L}{2}\right) - \left(\frac{R_{arm}}{2} * I_o + \frac{L_{arm}}{2}\frac{dI_o}{dt}\right) \quad (9)$$

$$V_{dc} = (V_U + V_L) + 2\left(R_{arm} * I_{dif} + L_{arm}\frac{dI_{dif}}{dt}\right) \quad (10)$$

2.3. MMC control systems

The MMC control scheme illustrated in Figure 3 is divided into two main components: outer power control and inner grid current control. The output power control determines the power exchange between the MMC and the AC grid. It provides the reference current levels that will be tracked by the inner grid current control. Given that the grid voltage and frequency at the point of common coupling are fixed, power is controlled by controlling the injected currents.

In addition to the modulation strategy, MMC specific control algorithms also exist. One such algorithm is the circulating current suppression control (CCSC), which mitigates the presence of second-harmonic currents in the arms. Circulating currents lead to underutilization of the SM current-handling capacity, higher power losses, and a requirement for larger heat sinks.

Another critical MMC-specific algorithm is the capacitor voltage sorting and balancing (CVSB). It ensures the equalization of all SM capacitor voltages within an arm. Failure to maintain a balance leads to SM divergence, resulting in extreme voltage breakdown in capacitors that are constantly charging, or voltage collapse in capacitors that are constantly discharging. Thus, the CVSB algorithm ensures safe and uninterrupted MMC operations.

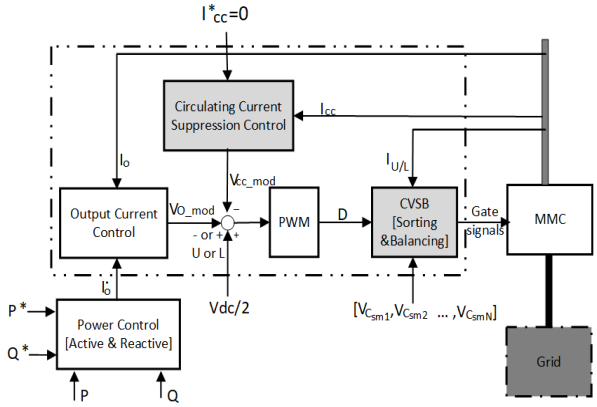

Figure 3: MMC control scheme

This study uses PI controllers for the MMC controls. To ensure the optimal performance of these controllers, it is necessary to transform AC quantities into the DQ coordinate system using Clark and Park transformations. This ensures the proper functioning of the controllers. Furthermore, the synchronization of the MMC with the ship grid is achieved through the utilization of a Phase-Locked Loop (PLL), which extracts the electrical angle from the grid voltage signals. We chose to align the grid voltage along the D-axis.

2.3.1. Output current control

Based on the single-line diagram in Figure 2 the equivalent circuit for the AC output current is shown in Figure 4.

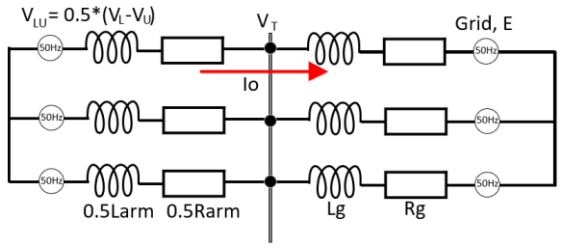

Figure 4: Equivalent circuit for the grid current

By deriving equation (11) from Figure 4, the design equation (12) for the control system in the ABC reference frame is obtained.

$$V_{LU} = \left(R_g + \frac{R_{arm}}{2}\right) * I_o + \left(L_g + \frac{L_{arm}}{2}\right) * \frac{dI_o}{dt} + E \qquad (11)$$

With $R = \left(R_g + \frac{R_{arm}}{2}\right)$ and $L = \left(L_g + \frac{L_{arm}}{2}\right)$,

$$\begin{bmatrix} V_a \\ V_b \\ V_c \end{bmatrix} = R * \begin{bmatrix} I_{o_a} \\ I_{o_b} \\ I_{o_c} \end{bmatrix} + L * \begin{bmatrix} \frac{dI_{o_a}}{dt} \\ \frac{dI_{o_b}}{dt} \\ \frac{dI_{o_c}}{dt} \end{bmatrix} + \begin{bmatrix} E_a \\ E_b \\ E_c \end{bmatrix} \qquad (12)$$

The equation (13) represents equation (12) in DQ coordinates.

$$\begin{bmatrix} V_d \\ V_q \end{bmatrix} = R * \begin{bmatrix} I_{o_d} \\ I_{o_q} \end{bmatrix} + L * \begin{bmatrix} \frac{dI_{o_d}}{dt} \\ \frac{dI_{o_q}}{dt} \end{bmatrix} + L\omega * \begin{bmatrix} -I_{o_q} \\ I_{o_d} \end{bmatrix} + \begin{bmatrix} E_d \\ E_q \end{bmatrix} \qquad (13)$$

The plant model for the output current can be obtained by applying the Laplace transform to the equation, resulting in equation (14).

$$\begin{bmatrix} V_d(s) \\ V_q(s) \end{bmatrix} = (R + sL) * \begin{bmatrix} I_{o_d}(s) \\ I_{o_q}(s) \end{bmatrix} + L\omega * \begin{bmatrix} -I_{o_q}(s) \\ I_{o_d}(s) \end{bmatrix} + \begin{bmatrix} E_d(s) \\ E_q(s) \end{bmatrix} \qquad (14)$$

To enable independent control of the D-axis and Q-axis currents, the coupling term $-L\omega I_{o_q}(s)$, $L\omega I_{o_d}(s)$ and the grid voltage values E_d and E_q are fed forward. By employing pole-cancellation techniques, the PI gains can be determined using the following equation:

$$K_{p\_c} = 2\pi L f_{bw}, \qquad (15)$$
$$K_{i\_c} = 2\pi R f_{bw}, \qquad (16)$$

In these equations, f_{bw} represents the controller bandwidth, which is typically set to 1/10th of the switching frequency.

2.3.2. Output power control

The output D and Q current references are determined based on active and reactive power controls respectively. Considering the chosen alignment of the grid voltage with the D-axis ($E_q = 0$), equation (17) represents the active power and equation (18) represents the reactive power.

$$P = \frac{3}{2}\left(E_d I_d + E_q I_q\right) = \frac{3}{2}\left(E_d I_d\right) \qquad (17)$$
$$Q = \frac{3}{2}\left(E_q I_d - E_d I_q\right) = -\frac{3}{2}\left(E_d I_q\right) \qquad (18)$$

2.3.3. Circulating current suppression

In an MMC, the second-harmonic circulating current primarily circulates within the converter itself. This has AC component of twice the fundamental frequency which must be suppressed. Figure 5 shows the equivalent circuit of the differential current. With $V_{cc} = V_u + V_L$

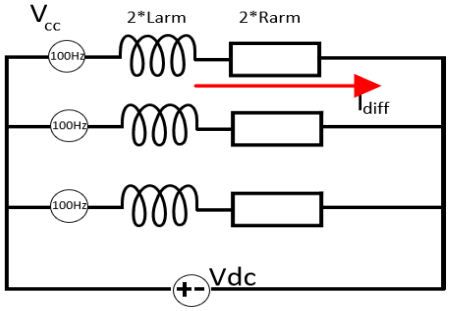

Figure 5: Equivalent circuit for differential current

The circulating current part of the differential current [100 Hz] is governed by equation (19).

$$V_{cc} = \left(R_{arm} * I_{cc} + L_{arm}\frac{dI_{cc}}{dt}\right) \qquad (19)$$

Given that the second harmonic is a negative sequence, the synchronization signal from the PLL is multiplied by -2 before the DQ transform. The circulating current plant model in DQ coordinates is given by equation (20).

$$\begin{bmatrix} V_{cc_d} \\ V_{cc_q} \end{bmatrix} = R_{arm}\begin{bmatrix} I_{cc_d} \\ I_{cc_q} \end{bmatrix} + L_{arm}\begin{bmatrix} \frac{dI_{cc_d}}{dt} \\ \frac{dI_{cc_q}}{dt} \end{bmatrix} + 2L_{arm}\omega * \begin{bmatrix} I_{cc_q} \\ -I_{cc_d} \end{bmatrix} \qquad (20)$$

The circulating current control equation is identical to that of the output current control. Pole placement was also used to tune the PI gains.

2.4. Modulation and arm capacitor voltage sorting and balancing (CVSB)

2.4.1. Modulation

Pulse width modulation (PWM) was used to translate the control output into gate signals. By adjusting the duty cycles of the switching devices, the targeted output can be achieved. MMC use multi-carrier modulation schemes (N carrier signals) such as phase-shifted carrier (PSC-PWM)

and level-shifted carrier (LSC-PWM) modulations. In PSC-PWM, triangular carrier signals with unity magnitudes but phase-shifted from one another are compared with the modulating signal. In LSC-PWM, triangular carrier signals with magnitudes equal to 1/N of unity are compared with the modulating signal. Another modulation technique used in this study is the nearest level modulation (NLM) which is based on approximating the insertion indices to the nearest step level based on the modulating signal.

2.4.2. Arm capacitor voltage sorting and balancing (CVSB)

To avoid the collapse of the MMC or the breakdown of capacitors due to the divergence of capacitor voltages, the capacitor voltages are strictly supervised and adjusted. The voltages are first read, sorted in ascending order, and then the SM to be switched are chosen based on their relative voltages, the current insertion index and direction of the arm current as shown in Figure 6. For any insertion index, D, if the arm current is positive, the D submodules with the least charged capacitors are switched on so that they can charge up, whereas for negative arm currents, the D submodules with the highest charged capacitors are discharged.

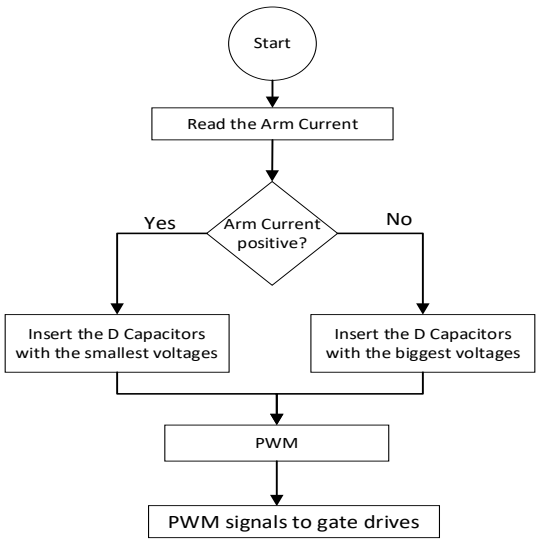

Figure 6: CVSB algorithm

3. CURRENT CAPACITOR VOLTAGE ESTIMATION METHODS FOR MMC.

Several methods have been proposed most of which rely on the state-space model of the MMC system. In [4] an adaptive back-stepping observer was proposed, whereas in [5] the authors used Kalman filter estimation. In [6], a sliding mode observer and state estimator were used, considering currents and capacitor voltages as state variables. In [7] the authors used an adaptive filter, but this time included capacitances as an uncertain parameter as capacitances of electrolytic capacitors may vary greatly. This increases the accuracy but also the complexity of the problem which has to be solved in near real time in order to provide the gate signals on time. In [8], an observer was directly integrated into model predictive control of the MMC. In [9] a modified sliding-mode observer was proposed.

Analytical methods based on SM states have also been proposed and have the advantage of being both simple and able to periodically correct the estimation errors by using real measurement data. In [10] and [11], the authors used the analytical expression of the capacitor voltage in equation (21). The total arm voltage was measured and compared to the sum of the estimated arm-capacitor voltages. The estimation error was then redistributed among all "on" state capacitors either equally or based on their duty cycles or their average switching function.

$$V_{c_{xyn}}(k+1) = \frac{1}{C_{sm}} \int_{t_k}^{t_{k+1}} S_{xyn}\, i_{xy} dt + V_{c_{xyn}}(k) \quad (21)$$

For this technique, refreshment with accurate values from arm voltage measurement only takes place when the insertion index (D) of the arm is one. At this index, the arm voltage equals the capacitor voltage of the SM in "on" state minus the small voltage drop across the active SM in the arm.

The validity of all the above-mentioned methods, and thus the accuracy and stability of the control loops built up on them depends on the accuracy of the underlying models used by these estimators. Often, these methods must pass through model linearization which reduce model fidelity. Furthermore, the model parameters are usually assumed to be constant, however, in reality, they fluctuate. In particular, observer-based methods provide a filtering property that estimates the states of variables values from their previous values and measurable outputs. They rely entirely on the mathematical model of the system and are thus very vulnerable to changes in parameters due to ageing or temperature changes. Analytical techniques on their part also rely on the accuracy of the model. However, this dependence can be eliminated using sufficiently high refreshment. For example, simple interpolation techniques other than the analytical equation of capacitor (dis)charging could be used between measurement points if the refreshment was sufficiently fast. As a matter of fact, analytical techniques amount to the digital equivalent of signal sampling and using

approximation techniques to estimate the values between samples. The higher the sampling rate, the better the quality of the reconstructed signal. However, the current methods have a low refreshing frequency, as this is only possible if the arm insertion index equals unity. That is, for an MMC with N+1 steps and period T, we have a window of less than d_1*T, where we can apply this technique, as shown in Figure 7 by the red window. d_1 is the arm duty cycle at unity insertion index. Furthermore, these refreshments are not uniformly distributed throughout the period, but are regrouped within the red band corresponding to the unity insertion index, as shown in Figure 7.

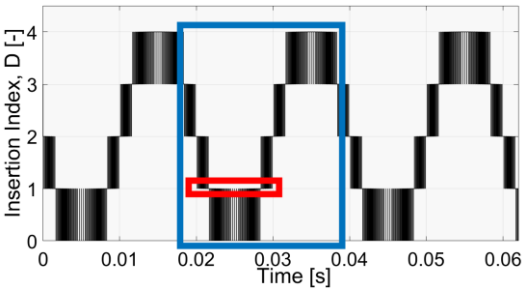

Figure 7: Insertion index of upper arm

Analytical techniques are a good option if a method can be found that increases the refreshment frequency and if these refreshments are uniformly distributed throughout the period irrespective of the insertion index. This is the purpose of the proposed method.

4. PROPOSED CAPACITOR VOLTAGE ESTIMATION

Unlike current analytical estimation algorithms, the proposed algorithm is a state transition-based technique that uses the change in the measured arm voltage and attributes it to a particular arm SM capacitor. Gate-state changes provide a unique identification of the SM.

As shown in Figure 7, the insertion index of an MMC changes by one under normal operation. This means that optimally, one SM goes on or off at any given time. Therefore, the change in arm voltage corresponds to the contribution of the SM. Given that switching occurs through the period and in the sub-second range, the refresh rate is high and distributed over most of the period on the insertion index graph, as shown by the blue window in Figure 7. For this algorithm, first the capacitor voltages were initialized. The signals from the gates were monitored to detect any state transitions. At any time, a state transition is retained if no other state transition is simultaneously detected. The SM undergoing the change is attributed the corresponding change in arm voltage minus a negligible voltage drop as illustrated in Figure 8.

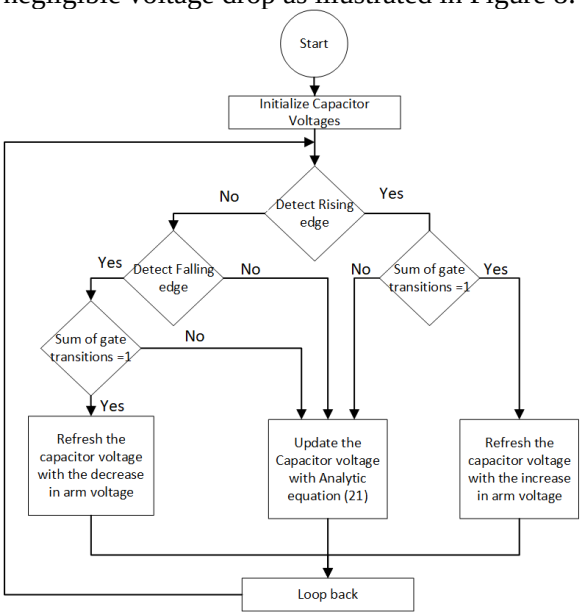

Figure 8: Proposed CVE algorithm

5. SIMULATION VERIFICATION

5.1. MMC simulation model

The performance of the proposed CVE was tested through simulations using MATLAB/Simulink software. The MMC test parameters are listed in Table 2. The sensor measurements were used as benchmarks.

Parameters	*Value*
DC link Voltage (kV)	10
AC grid RMS Voltage (kV)	3.54
AC grid frequency (Hz)	50
Submodule Capacitance (mF)	2
Arm inductance (mH)	1
Grid inductance (mH)	2
Switching frequency (Hz)	2000
Number of submodules per arm	4

Table 2: System Parameter

5.2. Results and discussions

5.2.1. Accuracy of the proposed method

The proposed CVE algorithm was analyzed in steady state condition using LSPWM and compared with sensor-based measurements. As shown in Figure 9, the estimated capacitor voltage matches that of the sensor-based method. The error reached up to 0.02 %.

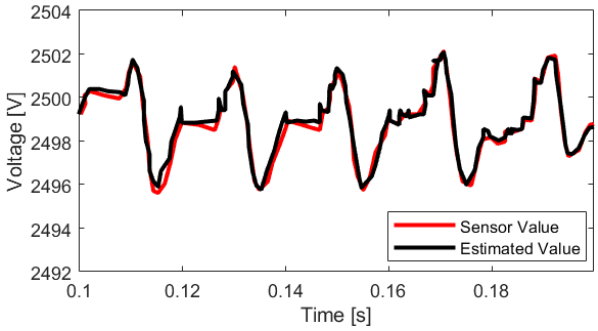

Figure 9: Proposed CVE performance

5.2.2. Dynamic performance in a closed loop

The proposed method was integrated into the MMC closed loop control. Figure 10 to Figure 13 show that the estimation seamlessly blends into the MMC controls. The proposed CVE estimation accuracy and speed were thus sufficient for MMC control. The settling time for the outer power controls are less than 0.1s as shown in Figure 10 and Figure 11. In Figure 12, the circulating current suppression control was triggered at the 0.1s thereby suppressing the 100 Hz currents in less than 0.03s. Figure 13 shows the output voltage and current of the converter. Figure 14 shows that the capacitor voltage for all the SM within the arms don't diverge meaning, the values provided by the proposed CVE estimation algorithm are sufficiently accurate to maintain stable operation in the CVSB block.

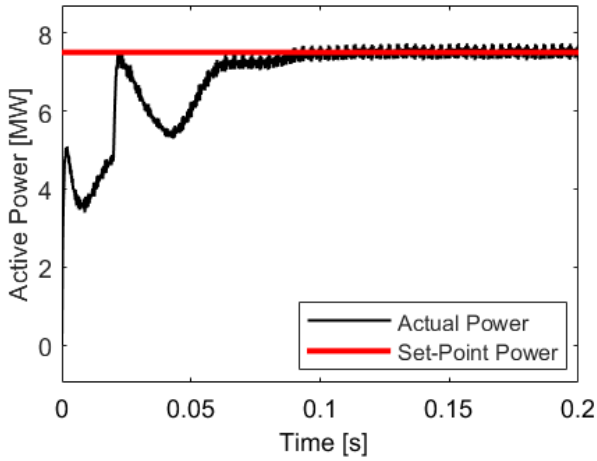

Figure 10: Active power controller time response

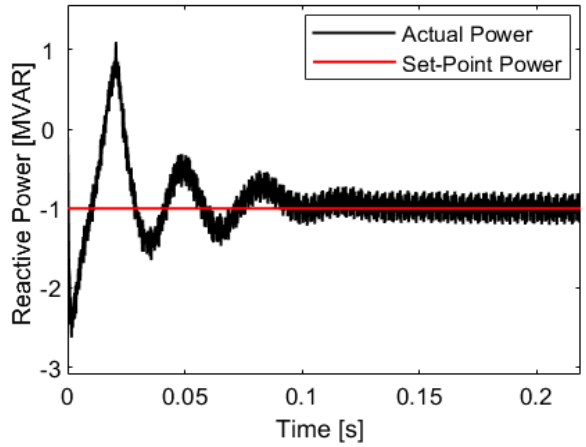

Figure 11: Reactive power time response

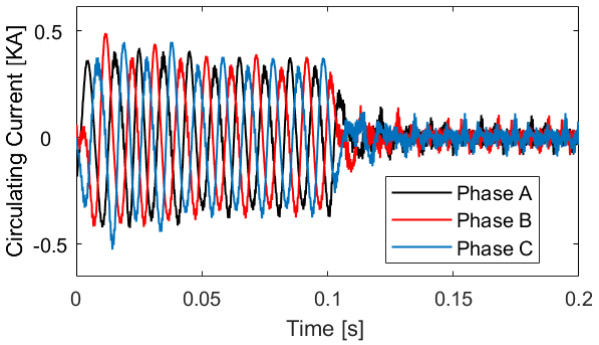

Figure 12: Circulating current suppression control

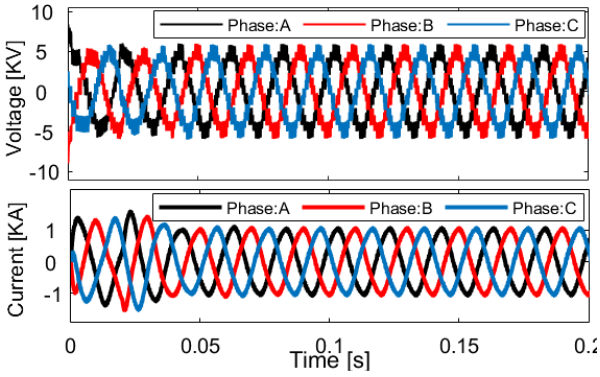

Figure 13: Converter output voltage and current

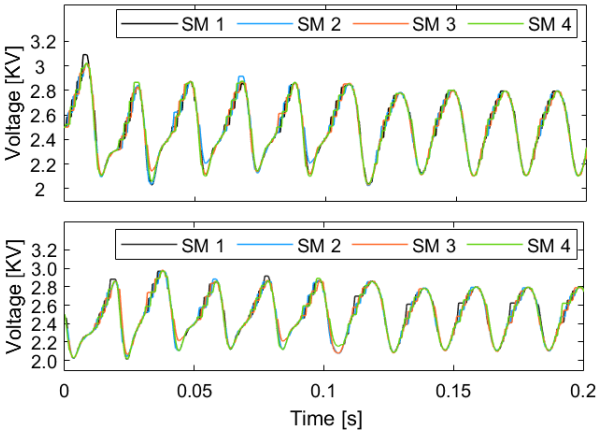

Figure 14: Capacitor Voltages for an MMC leg.

5.2.3. Performance evaluation under different conditions

The next step of the simulation studies involved studying the influence of different parameters on the tracking performance of the proposed CVE relative to the sensor-based method.

5.2.3.1. Influence of modulation type

As seen in the Figure 15 and Figure 160 for PSPWM and NLM, respectively, the tracking error is much reduced with the PSPWM scheme but much worse with NLM. This is because there is a natural balancing of capacitor voltages with the PSPWM technique, whereas the NLM technique needs the CVSB algorithm.

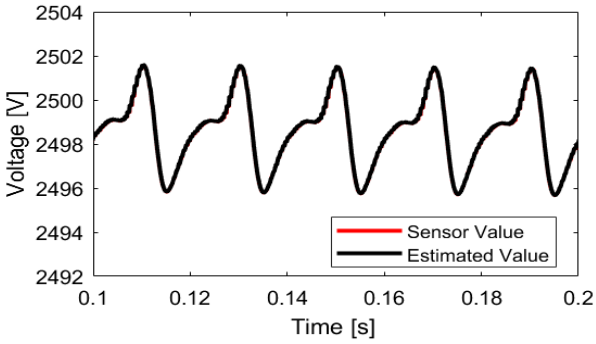

Figure 15: Sensitivity to modulation (PSPWM)

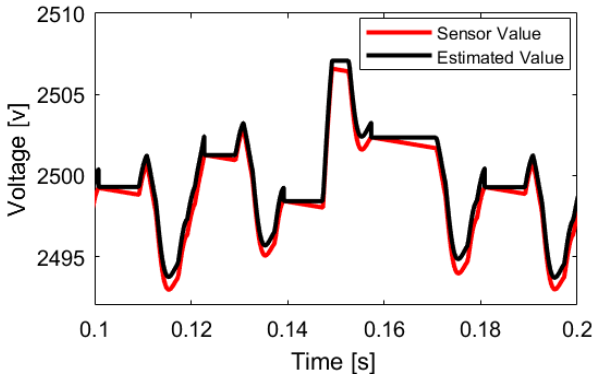

Figure 16: Sensitivity to modulation (NLM)

5.2.3.2. Influence of Switching frequency:

To investigate the effect of switching frequency, the LSPWM technique was utilized. It is seen that lowering the switching frequency still permits the estimation of the voltage although the error worsens as the switching frequency reduces as shown in Figure 17 and Figure 18 for switching frequencies of 600 Hz and 300 Hz respectively. The proposed algorithm is principally based on periodic reading of the arm voltage changes and attributing it to the changes in the submodule gate states meaning that the accuracy is improved if the arm voltage sampling frequency is increased. However, as seen from the different tracking errors, a high switching frequency does not necessarily lead to a large increase in tracking accuracy; on the other hand, it leads to an increase in switching power losses. However, high switching frequency also improve the harmonic content of the output AC voltage. The choice of the switching frequency is a compromise between the switching power losses, power quality, and voltage estimation accuracy.

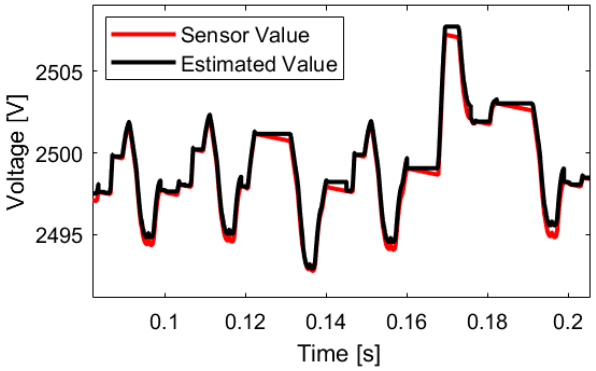

Figure 17: Effect of switching frequency (600Hz)

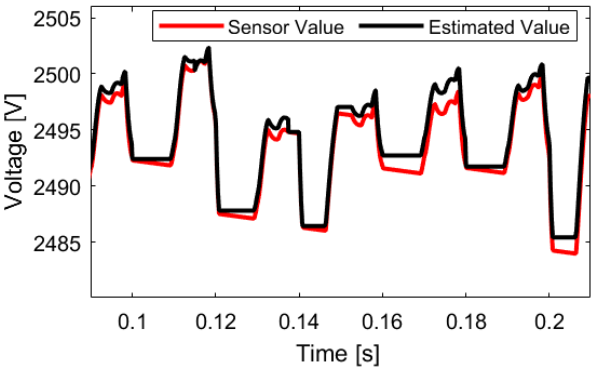

Figure 18: Effect of switching frequency (300Hz)

5.2.3.3. Influence of AC frequency:

At low AC frequencies, MMC usually underperforms as the capacitor voltages have longer charge/discharge periods, leading to the need for extra mitigation efforts in addition to the CCSC and CVSB. This is the case for MMC motor drives at low speeds. In the experiment, an RL load was used with a 5 Hz AC output. Figure 19 and Figure 20 show that compared to the sensor-based measurement, the proposed method is more accurate. This is because the proposed algorithm depends primarily on the switching frequency. The standard CVE algorithm used for comparison was the analytical technique employed in [10] and [11] as described in section 3 and depends on the unity

insertion index which in tend depends on the output AC frequency.

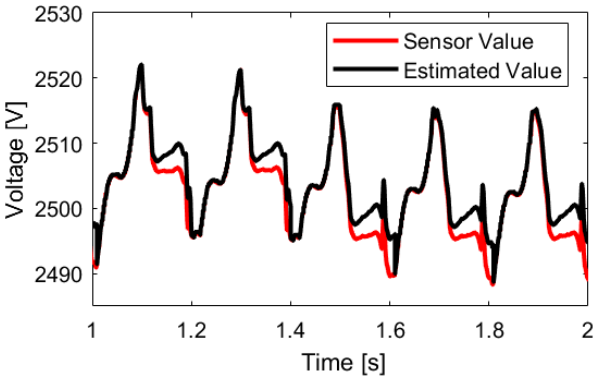

Figure 19: Standard CVE for low frequency AC.

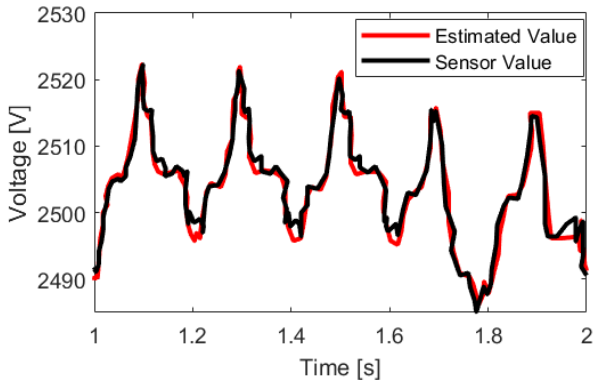

Figure 20: Proposed CVE for low frequency AC.

6. CONCLUSION

In this study, we propose an improved capacitor voltage estimation method for modular multilevel converters. The conventional method relies on a unity insertion index for estimation, which results in a long refresher time and limited accuracy, particularly in systems with a high number of submodules per arm. To address these limitations, we explored not only unity insertion index but also the transitions between successive insertion indices.

By utilizing the arm voltage at the transition points and the state changes of the switches, we developed an estimation algorithm that allows for periodic refreshing with measured data, thereby increasing the accuracy of the capacitor voltage estimation.

To validate the proposed method, we conducted a study on a four-submodule per-arm MMC system. The estimated capacitor voltages were compared with the sensor-based voltage measurements, confirming the validity of the proposed method. Furthermore, the proposed method was integrated into a complete MMC controller, including inner controls, such as circulating current and capacitor voltage balancing. Sensitivity studies were also conducted on different algorithm parameters and showed that the algorithm for a given switching frequency is immune to errors from model parameters, such as submodule capacitance, and also functions well at for low frequency applications.

The proposed capacitor voltage estimation method offers several advantages for MMC technology: by reducing the reliance on sensors, the method helps to decrease the number of potential points of failure and overall investment costs. Moreover, the improved accuracy of the voltage estimation contributes to enhanced system performance opening perspectives for operation under fault.

Though the proposed method thus provides a solution for a reliable and cost-effective capacitor voltage estimation in MMCs, the operation of the MMC critically relies on the availability of the arm voltage sensor and the accurate knowledge of the actual gate signals in near real time. Lack of data leads to faulty operations. Future research directions include extension to operation under fault conditions, further incorporation of the modified capacitor voltage sorting and balancing into the simulation to ensure cycling of all SM in the arms especially in fault operations. In addition, power hardware in the loop simulation on a test bench to validate this method will be the next step.

REFERENCES

[1] U. Javaid, F. D. Freijedo, D. Dujic and W. van der Merwe, "*MVDC supply technologies for marine electrical distribution systems*," in CPSS Transactions on Power Electronics and Applications, vol. 3, no. 1, pp. 65-76, March 2018, doi: 10.24295/CPSSTPEA.2018.00007

[2] L. Hong, Q. Xu, Z. He, F. Ma, A. Luo and J. M. Guerrero, "*Fault-Tolerant Oriented Hierarchical Control and Configuration of Modular Multilevel Converter for Shipboard MVdc System*," in IEEE Transactions on Industrial Informatics, vol. 15, no. 8, pp. 4525-4535, Aug. 2019, doi: 10.1109/TII.2018.2879981.

[3] G. Konstantinou, H. R. Wickramasinghe, C. D. Townsend, S. Ceballos and J. Pou, "*Estimation Methods and Sensor Reduction in Modular Multilevel Converters: A Review*," 2018 8th International Conference on Power and Energy Systems (ICPES), Colombo, Sri Lanka, 2018, pp. 23-28, doi: 10.1109/ICPESYS.2018.8626987.

[4] V. Najmi, H. Nademi and R. Burgos, "*An adaptive backstepping observer for modular multilevel converter*," 2014 IEEE Energy Conversion Congress and Exposition (ECCE), Pittsburgh, PA, USA, 2014, pp. 2115-2120, doi: 10.1109/ECCE.2014.6953682.

[5] O. Abushafa, S. Gadoue, M. Dhaidah and D. Aktinson, "*Capacitor voltage estimation in modular multilevel converters using a Kalman*

filter algorithm," 2015 IEEE International Conference on Industrial Technology (ICIT), Seville, Spain, 2015, pp. 3016-3021, doi: 10.1109/ICIT.2015.7125543.

[6] A. Al-Wedami, K. Al-Hosani and A. R. Beig, "*Sliding mode observer of submodular capacitor voltages in Modular Multilevel Converter*," 2015 International Workshop on Recent Advances in Sliding Modes (RASM), Istanbul, Turkey, 2015, pp. 1-6, doi: 10.1109/RASM.2015.7154650.

[7] H. Nademi, A. Das and L. E. Norum, "*Modular Multilevel Converter With an Adaptive Observer of Capacitor Voltages*," in IEEE Transactions on Power Electronics, vol. 30, no. 1, pp. 235-248, Jan. 2015, doi: 10.1109/TPEL.2014.2301879.

[8] M. Trabelsi, M. Ghanes, O. Ellabban, H. Abu-Rub and L. Ben-Brahim, "*An interconnected observer for modular multilevel converter*," 2016 IEEE Energy Conversion Congress and Exposition (ECCE), Milwaukee, WI, USA, 2016, pp. 1-7, doi: 10.1109/ECCE.2016.7854853.

[9] G. S. da Silva, R. P. Vieira and C. Rech, "*Modified sliding-mode observer of capacitor voltages in Modular Multilevel Converter*," 2015 IEEE 13th Brazilian Power Electronics Conference and 1st Southern Power Electronics Conference (COBEP/SPEC), Fortaleza, Brazil, 2015, pp. 1-6, doi: 10.1109/COBEP.2015.7420217.

[10] S. D'Arco and J. A. Suul, "Estimation of sub-module capacitor voltages in modular multilevel converters," 2013 15th European Conference on Power Electronics and Applications (EPE), Lille, France, 2013, pp. 1-10, doi: 10.1109/EPE.2013.6631931

[11] L. A. Grégoire, Weihua Wang, S. I. Seleme and M. Fadel, "*High reliability observers for modular multilevel converter capacitor voltage evaluation*," 2016 IEEE 8th International Power Electronics and Motion Control Conference (IPEMC-ECCE Asia), Hefei, China, 2016, pp. 2332-2336, doi: 10.1109/IPEMC.2016.7512661.

[12] L. A. M. Barros, A. P. Martins, and J. G. Pinto, "*A Comprehensive Review on Modular Multilevel Converters, Submodule Topologies, and Modulation Techniques*," Energies, vol. 15, no. 3, p. 1078, Feb. 2022, doi: 10.3390/en15031078.

[13] A. A. Ferreira, C. C.Rodríguez, and O. G. Bellmunt, "*Modulation techniques applied to medium voltage modular multilevel converters for renewable energy integration: A review*," in Proceedings of the Electric Power Systems Research, vol. 155, pp. 21-39, February 2018, doi: 10.1016/j.epsr.2017.08.015